A Herbig disk view of planet formation

Stapper, L.M.

Chapter 1

Introduction

From being subjects of mythology thousands of years ago, to helping us take our first steps towards understanding the universe around us: planets have played a significant role in our cultures and in our understanding of the universe since time immemorial. Particularly in the last few decades, modern technological progress has advanced astronomy in major ways. Not only are probes visiting planets in our Solar system, more than 5500 extrasolar planets have been confirmed to date. This enormous variety of exoplanets presents a challenge when it comes to understanding how planets form. The key in understanding this planet formation puzzle lies in protoplanetary disks, the nurseries of new exoplanets.

1.1 Star and planet formation

Star and planet formation is a complicated topic, spanning large ranges in space and time. Before a planetary system as we know it has formed, at least four different stages and millions of years have already passed.

The star formation cycle starts in a dense molecular cloud (see Fig. 1.1). This cloud mainly consists of gas, and some dust, with a typical gas-to-dust ratio of 100. Once dense and cold enough, the cloud starts to contract under its own gravity and collapse as it reached its so-called Jeans' mass. During this process, the density increases with a few orders of magnitude, from 10^2 hydrogen nuclei cm^{-3} to 10^6 cm^{-3} (Benson & Myers 1989). For the gas to be able to contract the temperature needs to stay low, around 10-15 K, which is aided by molecules radiating the heat away. The stages of star-formation have been formalized into four classes based on the slope of the infrared spectral energy distribution of the object,

$$\alpha_{\rm IR} = \frac{d \log \lambda F_\lambda}{d \log \lambda}. \tag{1.1}$$

The first three classes, Class I-III, were defined by Lada (1987), and later an earlier class, Class 0, was added by Andre et al. (1993), see Fig. 1.1. In between the Class I

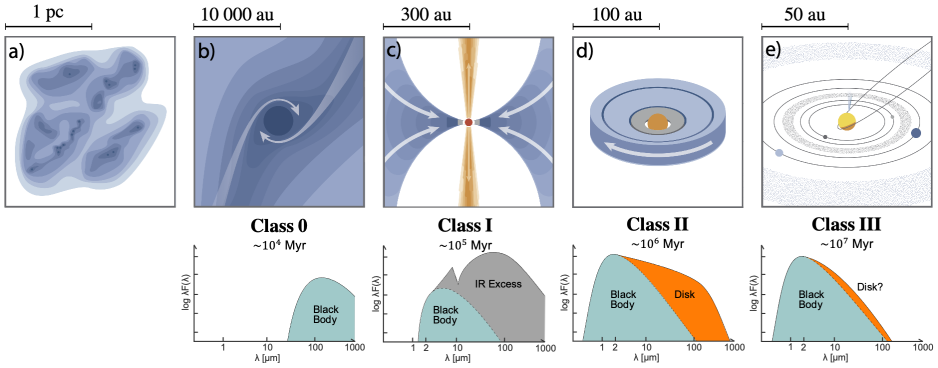

Figure 1.1: Star formation stages. **a)** Dense cores in interstellar molecular clouds. **b)** The cores start to collapse due to gravity, forming a protostellar core. This is a Class 0 object, and emits at long wavelengths. **c)** A protostar forms, still accreting from the remnant cloud, forming an accretion disk due to conservation of angular momentum. The emission from this Class I object consists of a star with additional IR excess from a disk and envelope. **d)** The remnant cloud dissipates and a disk is left over, a Class II object. The emission is dominated by the star and the disk. **e)** Eventually the primordial gas dissipates and a Class III object is left over, where stellar emission dominates. The typical size of the object is shown on top of the panels. Figure adapted from Öberg & Bergin (2021) and Magnus Persson.

and Class II stages, a flat spectrum source has also been defined (Greene et al. 1994).

Class 0 objects are still embedded in their envelope, making it difficult to observe the protostar at the center. Still, there is evidence of rotating gas disks in these young objects (e.g., Tobin et al. 2012; Murillo et al. 2013), which form due to conservation of angular momentum. The high accretion rates result in rapid evolution, and these embedded objects are therefore difficult to observe: protostars were first discovered through outflows of winds and jets (e.g., Snell et al. 1980; Codella et al. 2014; Bally 2016). When the envelope starts to dissipate, the star begins to be detectable and the object has transitioned to the Class I stage. As the disks of Class I objects are more massive than the successive classes, planet formation may already start at this stage (Tychoniec et al. 2020). Indeed, Class I objects show clear signs of disks with some already having visible substructures (ALMA Partnership et al. 2015; Sheehan & Eisner 2018; Segura-Cox et al. 2020). Once the envelope has dissipated and only a disk is left over, the Class II stage is reached. The disks of Class II objects, also called protoplanetary disks, have been subject of many detailed studies (e.g., Williams & Cieza 2011; Andrews 2020; Manara et al. 2023; Miotello et al. 2023), and are the focus of this thesis. Eventually, most of the disk has dissipated, either accreted onto the star, blown away by a disk wind, or formed into planets, and a debris disk is left over (Hughes et al. 2018). Planet formation is far from over in debris disks, as at this stage processes such as collisions and scattering between protoplanets (e.g., the Nice model, Tsiganis et al. 2005) are likely happening regularly. The dust and gas in

debris disks are thought to be secondary of nature, produced via these violent collisions (Hughes et al. 2018). When most of the disk has dissipated, a Class III object remains.

The pre-main sequence stars around which protoplanetary disks reside are often split into low and intermediate mass stars. The lower mass stars are called T Tauri stars, which have stellar masses lower than $\sim 1.5\ M_\odot$ and spectral types down to M. The disks around intermediate mass stars, further discussed in Sec. 1.4 and the focus of this thesis, reside around stars with a mass of ~ 1.5 to 8-10 $M_\odot$ with spectral types ranging from F to B (see Brittain et al. 2023, and Section 1.4). The disks around pre-main sequence intermediate mass stars are called Herbig disks.

1.2 Protoplanetary disks

1.2.1 Gas evolution

During the different stages mentioned in the previous section, disk evolution plays an important role. The evolution of the gas is thought to occur via two mechanisms: viscous evolution and/or driven by a magnetohydrodynamical (MHD) wind, see Fig. 1.2.

As the Keplerian rotation decreases with the square root of the radius, different annuli of the disk rotate with different velocities and the annuli shear against each other (Lynden-Bell & Pringle 1974). This process carries the angular momentum outwards, increasing the radius of the disk, while most of the material of the inner disk drifts inwards and is accreted by the star. This shear depends on the viscosity of the disk and is parameterized into the α-parameter (Shakura & Sunyaev 1973). Viscosity is assumed to be associated with turbulence in the disk, though this is not known with certainty, originating from for instance (magneto)hydrodynamical instabilities (e.g., MRI, Balbus & Hawley 1991; VSI, Nelson et al. 2013; see also

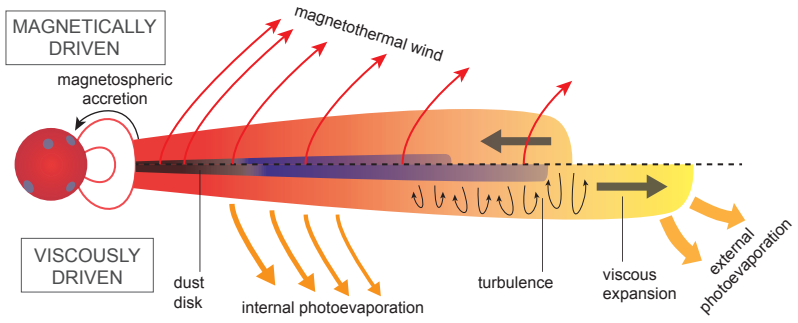

Figure 1.2: Schematic of the two main mechanisms thought to drive the evolution of the protoplanetary disk. While magnetically driven winds (top half) transport angular momentum away from the disk, decreasing the disk size, viscous evolution (bottom half) redistributes the angular momentum over the disk, increasing the disk size. Figure from Manara et al. (2023).

Bae et al. 2023 and Lesur et al. 2023). Based on this prescription the surface density of the disk can be described as

$$\Sigma_{\rm gas} = \frac{(2-\gamma)M_{\rm disk}}{2\pi R_c^2}\left(\frac{R}{R_c}\right)^{-\gamma}\exp\left[-\left(\frac{R}{R_c}\right)^{2-\gamma}\right], \tag{1.2}$$

if the viscosity ν is assumed to vary radially with the powerlaw $\nu \propto R^{\gamma}$ (Hartmann et al. 1998). Other parameters include the disk mass $M_{\rm disk}$, and the characteristic radius R_c, which is the radius at which the the exponential taper of the surface density profile takes over from the powerlaw part of the equation. As the turbulence is thought to be the driving factor behind viscous evolution, many works have tried to measure it. As of writing, the viscous parameter α is measured to be relatively low, in the order of 10^{-3}-10^{-5} (e.g., Flaherty et al. 2015, 2020; Villenave et al. 2022; Jiang et al. 2024), though some works estimate it to be higher (Hughes et al. 2011; Paneque-Carreño et al. 2024). Hence, it is still unknown what the main driver of the viscosity in disks is. Additional physical processes can be added, such as external or internal photoevaporation, which will influence the disk lifetime compared to an exclusively viscously evolving disk (see e.g., Rosotti et al. 2017).

Rather than the transport of angular momentum in the disk, MHD disk winds remove the angular momentum from the disk by using a magnetic field inherent to the disk. Recently, Tabone et al. (2022a) have parameterized the MHD disk evolution similar to the viscous case with an α_{DW}. With this parameterization, Tabone et al. (2022b) show that the fast dispersal and the correlation between the disk mass and accretion rate of the disks in Lupus can be reproduced with MHD disk winds (more on disk population studies, see Section 1.3). As material, and thus angular momentum, is removed from the disk, the disk radius stays the same or decreases with time (Trapman et al. 2022). Hence, the radius of the disk is one of the main observational signatures to distinguish MHD driven or viscous driven evolution.

1.2.2 Obtaining the gas mass

Besides the evolution of the gas in the disk, the total gas mass of the protoplanetary disk is also one of the most important open questions in the field of planet formation. Directly tracing the total disk mass is difficult; the most common molecule H_2 does not have a dipole moment, and its low-energy rotational levels are weak quadrupole transitions, which are faint at the low temperatures of the disk outer regions. The isotopologue of H_2, hydrogen deuteride (HD), however, does have a small dipole moment which allows for dipole transitions. The first rotational transition of HD $J = 1 - 0$ can be excited around 100 K and emits at 112 μm. This transition has only been detected with the *Herschel Space Observatory* for three disks (Bergin et al. 2013; McClure et al. 2016). For Herbig disks there are also a dozen of upper limits based on the HD measurements (Kama et al. 2016, 2020). Unfortunately, the *Herschel Space Observatory* ceased operations in 2013.

Therefore, (combinations of) other molecules need to be used as tracers for the total gas mass in disks. The most logical step is to use the second most abundant

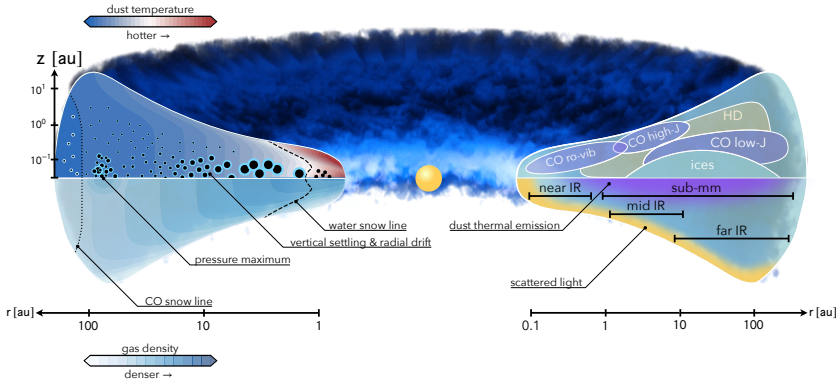

Figure 1.3: Schematic view of a protoplanetary disk. The left side of the figure shows the temperature and density structure of a disk. As the distance from the star increases, the temperature decreases, resulting in different molecules freezing out and giving rise to the snow lines (water close in, CO farther out). Dust grains grow via collisions, settle towards the midplane, and drift inwards due to gas drag. Pressure maxima in the disk can halt the radial drift at different radii. The right side shows the different parts of the disk which can be traced by different detection methods. The millimeter dust is observed at 10s of au near the midplane. Low rotational transition CO emission lines are emitted at higher regions of the disk. To trace the inner disk or the upper regions of the disk one needs to go towards IR wavelengths. Figure from Miotello et al. (2023).

molecule: carbon-monoxide (CO). Indeed, many works have used CO, or one of its many isotopologues (^{13}CO, C^{18}O, C^{17}O, ^{13}C^{18}O, ^{13}C^{17}O), to determine the total mass either by scaling the luminosity of the CO isotopologue using an excitation temperature and an abundance ratio (e.g., Hughes et al. 2008; Loomis et al. 2018; Miley et al. 2018), or using thermochemical models to obtain a disk mass by relating the luminosity of the disk to a particular model disk mass (Williams & Best 2014; Miotello et al. 2014, 2016). Other methods to obtain a disk mass include combining CO measurements with N_2H^+ (Trapman et al. 2022) or [OI] (Kamp et al. 2010) to try to solve degeneracies in the models such as the carbon abundance and the temperature of the disk.

To use carbon monoxide as a tracer of the total disk mass, two main processes need to be taken into account: photodissociation and freeze-out. Both processes impact the abundance of CO and therefore need to be treated carefully to obtain a gas mass from the CO emission. Photodissociation of CO occurs via the absorption of UV photons, as an energy of 11.09 eV is necessary, and proceeds through discreet lines into an excited electronic state. Therefore, at high enough column densities, CO can self-shield, as the UV absorption lines become optically thick. For rarer isotopologues such as ^{13}CO and C^{18}O self-shielding also occurs, in addition to the molecules mutually shielding each other as their UV absorption lines overlap

(Visser et al. 2009; Miotello et al. 2014). The self-shielding of each molecule is reached at different column densities in the disk, and therefore layers of different isotope ratios arise in the disk.

At a dust temperature of around 20 K, CO freezes out onto grains (Bisschop et al. 2006). This reduces the total amount of CO in the gas-phase, and therefore the brightness of the emission from the disk. However, even when taking the freeze-out into account, CO is found to be less bright than expected, resulting in low disk masses and gas-to-dust ratios of around 10 (e.g., Pascucci et al. 2016; Long et al. 2017; Miotello et al. 2017). Processes such as ice chemistry turning CO into molecules such as CO_2 and CH_4 (or more complex molecules such as CH_3OH) are therefore likely to be fundamental in understanding the CO emission (Bosman et al. 2018; Agúndez et al. 2018). Indeed, taking these processes into account results in an order of magnitude higher gas-to-dust ratios (Deng et al. 2023). Additionally, the CO ice can be locked into larger bodies in the midplane, removing it from the gas reactions higher up in the disk (Du et al. 2015; Krijt et al. 2018). In warm disks such as those around the more luminous Herbig stars the freeze-out of CO is much less relevant (Kama et al. 2020; Sturm et al. 2022; Miotello et al. 2023). For some Herbig disks evidence even suggests that no CO snow line is present (e.g., HD 100546, Kama et al. 2016). Therefore, CO can be used as a gas mass tracer in Herbig disks.

Lastly, both the freeze-out and photodissociation of CO results in CO being abundant between two boundaries in the vertical direction of the disk (see Fig. 1.3). The upper boundary set by the photodissociation from UV photons from the central star or an external field, while the lower boundary is set by the freeze out in the cold midplane of the disk (Aikawa et al. 2002), see Fig. 1.3.

For the modeling of the gas and chemistry of protoplanetary disks, multiple codes have been developed over the years, such as ProDiMo (Protoplanetary Disk Modeling, Woitke et al. 2009), and DALI (Dust And LInes, Bruderer et al. 2012; Bruderer 2013; Bruderer et al. 2014). For DALI, detailed CO chemical networks have been developed, including isotopologue specific photodissociation, mutual- and self-shielding, and freeze-out (Miotello et al. 2014, 2016). The isotopologue ratios are initiated with the ISM abundances (Wilson & Rood 1994). DALI then obtains the disk gas and dust thermal structure, and the abundances of each molecule in the disk by doing the following steps (see also Bruderer et al. 2012). First, using a specific density structure, see eq. (1.2), and a stellar spectrum, DALI obtains the dust temperature and UV radiation field in the disk. Then, the chemical network is run using the dust temperature as a first guess to the gas temperature, resulting in molecular abundances. Subsequently, the excitation of the molecules is calculated using non-LTE methods, providing the cooling rates. The gas temperature is then obtained from the balance between heating and cooling processes. This new gas temperature is then used to recalculate the chemistry and the molecular excitations. This process is iterated until they converge. DALI has been used in many different studies. From disk specific modeling (e.g., van der Marel et al. 2016; Leemker et al. 2021, 2022), to population studies (e.g., Miotello et al. 2016, 2017; Kama et al. 2020; Trapman et al. 2019).

1.2.3 Vertical structure of the disk

The gas can be used to trace other processes as well, especially with the velocity resolution of ALMA. CO emission profiles can reveal the kinematics in disks, showing minute changes in the 10s of m s^{-1} caused by possible embedded planets (e.g., Pinte et al. 2018b, 2019; Izquierdo et al. 2022; Wölfer et al. 2023). Similarly, the vertical height can be traced by using the isovelocity curves of the gas emission (Pinte et al. 2018a). As the gas is pressure supported, the gas will follow the rotation of the disk elevated from the midplane, resulting in a cone shape. From this shape the emission height can be inferred. This technique has been used to show clear vertical stratification of different molecules in the disk (e.g., Paneque-Carreño et al. 2023). The focus of this technique has mostly been on the CO isotopologues, with ^{12}CO, ^{13}CO, and C^{18}O $J = 2 - 1$ emitting from layers at an aspect ratio of $\sim 0.2 - 0.3$ and lower depending on the rarity of the isotopologue and where the emission line becomes optically thick (e.g., Law et al. 2021, 2022, 2023). Additionally, the vertical thermal structure of the disk can be inferred from the brightness temperature of the different layers (Law et al. 2021).

1.2.4 Dust evolution and planet formation

While the gas is evolving, the dust is too. As the dust will eventually form the (cores of) planets, this evolution is just as important as the evolution of the gas. The dust will settle vertically, drift radially, collide with other particles, and possibly be trapped in the disk (see Fig. 1.3). One of the most important findings by ALMA in the last decade is the presence of dust rings and other structures in protoplanetary disks. After the first confirmation of rings in HL Tau in 2015 (ALMA Partnership et al. 2015), others were soon to follow. The ALMA large program 'Disk Substructures at High Angular Resolution Project' (DSHARP, Andrews et al. 2018a) has shown a plethora of structures in the brightest disks. The disks show clear signs of dynamical processes occurring in them: ranging from rings and gaps (Andrews et al. 2018a), large cavities (Pineda et al. 2019; Benisty et al. 2021), crescents (Dong et al. 2018; Kraus et al. 2017; van der Marel et al. 2013), to spirals (Pérez et al. 2016). Many barriers need to be overcome to eventually form planets, but the timescale of planet formation is short, as disks disperse after only < 10 Myr (Haisch et al. 2001; Hillenbrand 2005). Still, we know that planets do form in disks: besides the thousands of detected exoplanets, which had to form somewhere, direct detections of young protoplanets in disks have been made as well (PDS 70, Keppler et al. 2018; Haffert et al. 2019; AB Aur, Currie et al. 2022; HD 169142, Hammond et al. 2023).

The dust evolution starts with small micron-sized dust coupled to the gas. This dust can be observed in scattered light (see Fig. 1.3, and for a recent overview Benisty et al. 2023). The gas is pressure supported resulting in a sub-Keplerian rotation velocity, which the small micron-sized dust follows. Based on the scattered light, these micron-sized particles have been inferred to be both low- and high-porosity aggregates, possibly linked to planets in the disk stirring up the more compact grains from the midplane (Ginski et al. 2023; Tazaki et al. 2023). If these grains are growing by sticking together, they need to overcome the bouncing

barrier (Zsom et al. 2010), which may be possible outside the snowline where the dust particles are more sticky due to an icy layer. Eventually, these small dust grains start to grow to centimeter or even decimeter sized particles, called pebbles, and decouple from the gas. Still, difficulties remain for overcoming the subsequent fragmentation barrier, where particles start to fragment instead of stick when colliding (e.g., Booth et al. 2018). A more direct mechanism to form planetesimals is via gravitational collapse triggered by the streaming instability (Youdin & Goodman 2005), due to the particles settling down in the midplane (Johansen et al. 2014), practically skipping the different barriers. The problem of radial drift may still remain however, which is caused by the pebbles experiencing a headwind due to the sub-Keplerian velocity of the pressure-supported gas. This headwind slows down the particle and it drifts inwards, which, based on dust evolution models, can happen on timescales of only a few 100 years (Pinilla et al. 2022b). To overcome this loss of grains, a pressure maximum is needed, where the particles will drift towards and be trapped. To make such a dust trap, many different mechanisms have been put forward. For example planets may directly form via gravitational instabilities in the outer disk (Boss 1997; Kratter et al. 2010), which will then generate spirals trapping the dust, and create dust traps of their own (e.g., Bae et al. 2017), kickstarting the dust growth for other planets. Other possible origins include snowlines (e.g., Zhang et al. 2021) or MHD zonal flows (e.g., Hu et al. 2022).

Eventually planetesimals will form, which then need to grow towards young protoplanets. The two main mechanisms proposed for this are planetesimal accretion and pebble accretion. For planetesimal accretion, the process is governed by gravity, as the planetesimals themselves are decoupled from the gas (Lissauer 1993; Kokubo & Ida 1996; Drążkowska et al. 2023). When the random velocities between the planetesimals is much smaller than the escape velocity, gravitational focusing dominates and a runaway growth starts. This will stop when the planet embryo is massive enough to dynamically stir the smaller planetesimals (Drążkowska et al. 2023). Unfortunately, the efficiency of planetesimal accretion drops with the separation from the star. Forming a massive planetary core outside the snowline takes therefore too long compared to the disk lifetime (Ida & Lin 2004). Pebble accretion may be a solution to this, where the planetesimal accretes smaller particles, pebbles, to grow (Visser & Ormel 2016; Johansen & Lambrechts 2017). As this process is assisted by the gas drag, material from a substantially larger radius can be accreted onto the planetesimal, making this process orders of magnitude faster than planetesimal accretion. But a large enough reservoir of pebbles is needed to be able to do so (Ormel 2017). Once the planetary core has been sufficiently built up, gas accretion starts. Consequently, the Bondi radius (the radius at which the sound speed of the gas equals the escape velocity of the embryo) extends and even more gas is accreted. A run-away growth period occurs, leading to a giant exoplanet forming (e.g., Pollack et al. 1996).

1.2.5 Obtaining the dust mass

The amount of dusty material as building blocks of planets is thus an important factor in the formation of exoplanets. To obtain a measure of the dust mass in a disk, often a relatively simple formulation is used (Hildebrand 1983),

$$M_{\rm dust} = \frac{d^2 F_\nu}{\kappa_\nu B_\nu(T_{\rm dust})}, \tag{1.3}$$

which assumes the dust to be optically thin. Here, the continuum millimeter flux F_ν is scaled to a dust mass $M_{\rm dust}$ via the distance d and by assuming a particular dust temperature $T_{\rm dust}$ and the Planck curve at that temperature B_ν. The dust temperature is often assumed to be 20 K for T Tauri disks (e.g., Andrews & Williams 2005), but the temperature can also be scaled with the luminosity of the central star (Andrews et al. 2011). The dust opacity κ_ν is assumed to be a powerlaw of the form (Beckwith et al. 1990)

$$\kappa_\nu = \kappa_0 \left(\frac{\nu}{\nu_0}\right)^\beta = 10 \text{ cm}^2 \text{ g}^{-1} \times \left(\frac{\nu}{10^3 \text{GHz}}\right)^\beta, \tag{1.4}$$

such that at a typical frequency of 230 GHz in Band 6 with ALMA, assuming the powerlaw index β to be equal to 1, the dust opacity is 2.3 cm^2 g^{-1}. However, β is not necessarily equal to 1, as it is related to the growth of the dust in the disk. Lower values are associated with dust growth. To obtain an estimate of the powerlaw index, observations at different wavelengths are needed. For example Tazzari et al. (2016) obtained $\beta = 0.5$ for the inner disk, and $\beta = 1.7$ for the outer disk (consistent with the ISM value of 1.8, Draine 2006) by combining VLA, SMA, and CARMA observations. Similar disk averaged values of $\beta = 0.5$ were found by Tychoniec et al. (2020) and Tazzari et al. (2021). Another uncertainty in obtaining a dust estimate is the assumption of optically thin emission. This may not be true, and dust masses may be underestimated by an order of magnitude, based on dust radiative transfer modeling using RADMC-3D (Dullemond et al. 2012; Liu et al. 2022) and MCFOST (Pinte et al. 2006, 2009; Kaeufer et al. 2023).

1.3 Disk population studies

In the past decade ALMA and other millimeter arrays have given the opportunity to obtain large samples of millimeter observations of protoplanetary disks, specifically to obtain their dust mass and radius. This section will summarize those results, after introducing two millimeter interferometers mainly used in this thesis.

1.3.1 Observing planet formation with millimeter interferometers

Interferometers are a collection of telescopes, or antennas, which combine their inputs into a single image. This effectively results in a telescope with a resolution

proportional to the largest separation (or baseline) between the antennas. As radio waves are combined, the array of antennas samples a Fourier transform of the sky brightness. These samples are called visibilities. As not all space between the telescopes is covered, there is a finite sampling of the visibilities. This results in artifacts in the 'dirty' image, due to the so-called point-spread function of the telescope, which need to be deconvolved out of the dirty image to obtain a cleaned image of the sky brightness.

The Netherlands has been at the forefront in radio astronomy for decades by building arrays such as the Westerbork Synthesis Radio Telescope (WSRT), and the Low-Frequency Array (LOFAR). For planet formation however, we need to look at millimeter wavelengths, as planet-forming disks radiate at these wavelengths. While for radio telescopes the Dutch weather is not a big problem, for shorter wavelengths dryer conditions are required. One of the world leading observatories is therefore located in the Atacama desert in the Andes mountain range in Chile at a height of 5000 m above sea level: the Atacama Large Millimeter/submillimeter Array (ALMA). ALMA is an international partnership between Europe, North America, east Asia, and the Republic of Chile. The array consists of 66 antennas, of which 54 have a diameter of 12 meters, and 12 have a diameter of 7 meters. Part of ALMA is the so-called Atacama Compact Array (ACA), which consists of 16 closely separated antennas: the 12 7-meter antennas together with 4 12-meter antennas. The antennas can be arranged into different configurations, changing their baselines from 150 meters all the way to 16 kilometers. The largest separations can give milli-arcsecond (mas) resolution at the highest frequencies observed. Additionally, ALMA has a high velocity resolution as well, being able to resolve emission lines at a velocity resolution of only 50 m s^{-1}.

Another millimeter interferometer, though less often used for planet formation than ALMA, is the Northern Extended Millimeter Array (NOEMA). This telescope is located on Plateau de Bure in the French Alps at a height of 2500 meters. NOEMA is operated by the Institut de Radioastronomie Millimetrique (IRAM) which is supported by institutes in France, Germany, and Spain. This array consists of 12 15-meter antennas. At its most extended configuration the baselines can range out to 1.7 kilometers. The main strength of NOEMA is its large bandwidth. Its upper and lower side-band are 8 GHz wide, making it particularly useful for molecular emission line surveys. In addition, while the spatial resolution and sensitivity do not match that of ALMA, it can be nicely used for photometric surveys as its beam size (resolution) matches with the size of planet-forming disks in the nearby star-forming regions, optimizing the sensitivity for those kinds of observations.

The unique features of both telescopes allow for large surveys of planet-forming disks in relatively short integration times. In particular ALMA has revolutionized star and planet formation since the telescope saw its first light in 2011. It has been used extensively to obtain large samples of disks (nearly 2000 in total) around pre-main sequence stars in nearby low-mass star-forming regions such as Lupus, Taurus, Chamaeleon, and Upper Sco, and high-mass star-forming regions such as Orion.

Figure 1.4: The 12 meter antennas of the Atacama Large Millimeter/submillimeter Array (ALMA, top), and the 15 meter antennas of the Northern Extended Millimeter Array (NOEMA, bottom). Credit: ESO/C. Malin, and IRAM.

1.3.2 Findings from population studies

Protoplanetary disk population studies have greatly advanced our understanding of planet formation in the past decade. Different relationships between parameters have been found, which will be discussed here. A recent review by Manara et al. (2023) has collected the data of seven nearby star-forming regions, see Fig. 1.5. These star-forming regions include: Ophiuchus (Cieza et al. 2019; Williams et al. 2019), Taurus (combination of ALMA and SMA observations, e.g., Andrews et al. 2013, see Manara et al. 2023 for more details), Lupus (Ansdell et al. 2016, 2018; Sanchis et al. 2020), Chamaeleon I (Pascucci et al. 2016; Long et al. 2018), Chamaeleon II (Villenave et al. 2021), Upper Scorpius (Carpenter et al. 2014; Barenfeld et al. 2016; van der Plas et al. 2016), and Corona Australis (Cazzoletti et al. 2019). Besides these nearby star forming regions, Orion has been subject of many studies as well. One of the largest surveys to date is of L1641/L1647 (SODA, van Terwisga et al. 2022; van Terwisga & Hacar 2023), consisting of 873 disks in total (see also Grant et al. 2021). Other regions surveyed in Orion include σ Orionis (Ansdell et al. 2017), λ Orionis (Ansdell et al. 2020), NGC 2024 (van Terwisga et al. 2020), the Orion Nebula Cluster (ONC, Eisner et al. 2018), and the Orion Molecular Cloud-2 (van Terwisga et al. 2019). This section will shortly summarize some of the relationships found for the disk dust mass from these population studies, for a more comprehensive overview see Manara et al. (2023).

1.3.2.1 Dust mass versus stellar mass and age

One of the main findings from disk populations is the relationship between the stellar mass and the disk dust mass. Before ALMA, this relationship was already reported by Andrews et al. (2013) for the Taurus region. Since then, many other population studies done the same for other regions. The left panel of Figure 1.5 shows the disk dust and stellar masses of seven star-forming regions as collected by Manara et al. (2023).

Combining all surveys into one figure does not immediately show that there is a trend between the dust mass and stellar mass. However, when looking at each region separately, this relationship is well established by now. When fitting a powerlaw through the relation, $M_{\rm dust} \propto M_{\rm star}^{\alpha}$, the powerlaw index α was found to range from 1.7±0.2 for the 1-2 Myr old Taurus region to 2.4±0.4 for the 5-11 Myr old Upper Sco region, with in between values of α for regions with intermediate ages (Ansdell et al. 2017). These relationships have also been added to the left panel of Fig. 1.5. Around the relationship a spread of 0.6-0.9 dex is present, likely related to the initial formation conditions of the disks as this spread is present for all ages (Manara et al. 2023).

While tentative, the relationship between the stellar mass and the disk dust mass seems to steepen over time: the higher mass disks retain their disk mass for longer. While this particular relationship has not been subject of many modeling studies, the steepening of the relationship may be due to the effect of dust traps stopping radial drift (Pinilla et al. 2020). As the dust is stopped at larger radii, the emission area is larger and thus the recovered disk mass is higher. Still, the overall mass budget in millimeter sized grains clearly decreases in time, see Figure 1.6. This is likely due to disk dispersal, or grain growth and/or evolution (Manara et al. 2023). Though trends with age must be looked at carefully, as contamination due

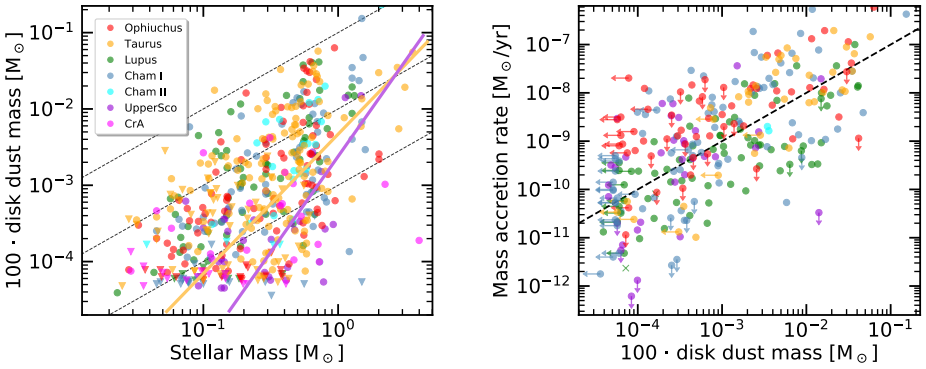

Figure 1.5: Relationships found based on the disk populations done with ALMA. The left panel shows the disk dust mass, stellar mass relationship, with the relationships for Taurus and Upper Sco from Ansdell et al. (2017) overplotted. The right panel presents the mass accretion rate against the disk dust mass. Both panels are from Manara et al. (2023).

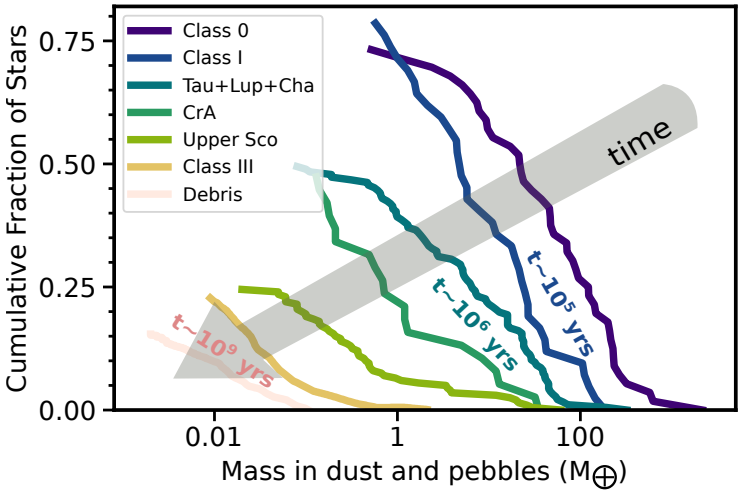

Figure 1.6: Dust mass cumulative distribution from Class 0 objects to debris disks from Drążkowska et al. (2023). There is a clear decrease in total disk mass, and fraction of stars with a disk, seen over time.

to the complex history of the region may happen (e.g., Krolikowski et al. 2021).

1.3.2.2 Versus disk dust radius

A relationship between the disk dust radius and the disk luminosity (or disk mass) has been found as well (Andrews et al. 2010; Tripathi et al. 2017; Tazzari et al. 2017, 2021; Hendler et al. 2020; Sanchis et al. 2021). The relationship is generally found to be sub-linear with a slope of $\sim$ 0.5 (ranging from 0.4-0.6) in Lupus, Chamaeleon I, Ophiuchus, and Taurus, while for Upper Sco a shallower slope of $\sim$ 0.2 was found (Hendler et al. 2020). One interpretation of this relationship is the presence of optically thick substructures in the disks (Tripathi et al. 2017; Andrews et al. 2018b; Zormpas et al. 2022). As the dust radial drift is stopped by the substructures, the emission size of the disk stays large.

A difference between the dust and (CO) gas radius has been found as well. While appealing, the difference cannot solely be related to radial drift. The optical depth of the dust continuum and gas lines differ: the continuum emission will be below the detection limit at smaller radii compared to the optically thick CO emission (Guilloteau & Dutrey 1998; Facchini et al. 2017; Trapman et al. 2019). A combination of optically thick gas emission and radial drift is indeed necessary to explain the ratio of $\sim$ 2 between the gas radius and dust radius found for the disks in Lupus (Ansdell et al. 2018).

1.3.2.3 Versus stellar accretion rate

The relationship between the accretion rate and dust mass is well established and much more similar between different star forming regions compared to the stellar mass dust mass relationship, see the middle panel of Fig. 1.5. The accretion rate $\dot{M}_{acc}$ increases close to linearly with disk dust mass, which is expected from viscous evolution models (Manara et al. 2016; Rosotti et al. 2017). The spread of the relationship is distributed around the $M_{\rm disk}/\dot{M}_{\rm acc} = 1$ Myr line. From viscous evolution, this spread is expected to decrease with time, as the high and low accretors are decreasing in disk mass at different rates. This is however not observed in Upper Sco (Manara et al. 2020), but can be solved by taking into account that many of these disks are radial drift dominated and are therefore compact and some of the mass is not accounted for (Sellek et al. 2020). Other factors impacting the relationship between the stellar accretion and disk dust mass are for instance stellar irradiation and photo-evaporation (Rosotti et al. 2017), giant planets (Manara et al. 2019a), and binarity (Zagaria et al. 2022). Lastly, while the relationship is expected from viscous evolution, MHD disk winds can also explain the seen relationship and corresponding spread (Tabone et al. 2022b).

1.3.3 Comparisons to exoplanets

As large numbers of disks and exoplanets start to be gathered, comparisons between the two can be done. These comparisons have shown that the amount of dust present in Class II disks is less than what is necessary to build the exoplanetary systems observed (Manara et al. 2018; Tychoniec et al. 2020), though a careful consideration of the detection biases in the exoplanet population suggests that it is more similar (Najita & Kenyon 2014; Mulders et al. 2021). This can be reconciled by letting planets already form early on in the lifetime of the disk. Tychoniec et al. (2020) show that in Class 0 and I objects there is enough mass for the seen planet population to be formed. Indeed, recent observations show that dust substructures are already present in Class I objects (e.g., ALMA Partnership et al. 2015; Sheehan & Eisner 2018; Segura-Cox et al. 2020). van der Marel & Mulders (2021) demonstrate that the fraction of structured disks is strongly dependent on stellar mass, and that the occurrence rate of giant exoplanets is the same as the frequency of structured disks. This suggests a relation between giant exoplanets and the structures seen in disks. Furthermore, planets smaller than Neptune are anti-correlated with stellar mass, and are likely related to the non-structured disks (Mulders et al. 2015; van der Marel & Mulders 2021). These more compact disks are more likely to form Super-Earths due to a higher pebble flux (Lambrechts et al. 2019).

1.4 Planet formation around intermediate mass stars

The population studies discussed above have given important insights into the evolution of disks around pre-main sequence stars. However, as the stellar mass increases fewer stars reside in each star-forming region, at most only a couple

of intermediate mass stars are present in each. Therefore a dedicated study on intermediate mass stars is missing, which this thesis aims to solve.

1.4.1 What are Herbig stars?

Herbig Ae/Be stars were first observed in the seminal paper of George Herbig (Herbig 1960), who selected 26 Ae and Be stars which lie in obscured regions and illuminate nearby luminosity, trying to find stars with masses ranging from 3 $M_\odot$ to 20 $M_\odot$. Since then, the definition of a Herbig star has evolved. Herbig Ae/Be stars are defined as having spectral types B, A, and F, hydrogen emission lines (hence the "e"), and an infrared excess (The et al. 1994; Malfait et al. 1998; Waters & Waelkens 1998; Vieira et al. 2003; Brittain et al. 2023). The stellar masses range from 1.5 $M_\odot$ to 10 $M_\odot$, with the upper limit set by the stellar mass for which a non-obscured pre-main sequence phase is still expected (Brittain et al. 2023). The lower limit on the stellar mass on the other hand is set by the coolest (i.e., latest spectral type) star which is thought to reach the zero age main sequence as an A9 star. Therefore, as the star evolves towards the main sequence, there are stars which look like T Tauri stars but are of intermediate mass. These stars are called Intermediate Mass T Tauri stars and have spectral types of F0 to K3 and stellar masses ranging from 1.5 to 5 solar masses (Calvet et al. 2004; Valegård et al. 2021).

Thanks to ESA's Global Astrometric Interferometer for Astrophysics (Gaia) space observatory (Gaia Collaboration et al. 2016), the parallaxes to stars have been accurately obtained for more than 1.5 billion stars. By using the accurate parallaxes from Gaia data release 2 (Gaia Collaboration et al. 2018a), Vioque et al. (2018) obtained the distances and stellar parameters such as the stellar luminosities, masses, and ages of 252 Herbig stars. More recently, Gaia early data release 3 parallaxes (Gaia Collaboration et al. 2021) have also been used (Guzmán-Díaz et al. 2021). Based on these works, there are a total of 31 Herbig stars known within 225 pc and 87 Herbig stars within 450 pc (Guzmán-Díaz et al. 2021). However, these sets of Herbig stars are likely to be influenced by historical biases. Hence, Vioque et al. (2022) added 128 new Herbig stars based on new optical spectroscopy data, mostly residing at distances larger than 600 pc, making the total number of known Herbig stars to be around 360. Machine learning may identify even more (Vioque et al. 2020). In addition to the Herbig stars, the Gaia astronometric data have also been used to obtain a total of 49 Intermediate Mass T Tauri stars (Valegård et al. 2021). While being the precursors of Herbig stars, these stars need to be included for a complete view of disks around pre-main sequence intermediate mass stars.

Herbig stars are Class II objects, this is mainly due to part of its definition: the hydrogen emission lines necessitate that the Herbig stars are accreting and optically visible and therefore a mostly unobscured disk needs to be present. Removing this definition and only looking at the pre-main sequence intermediate mass stars which have an infrared excess (down to debris disk levels) reveals that a significant fraction of these stars have only debris disks left (Iglesias et al. 2023). Even though Herbig stars are relatively old, with a median age of a Herbig Ae star being 6 Myr, large and massive disks are still the norm (see Section 1.4.3).

Work towards a complete inventory of all intermediate mass pre-main sequence stars and their disks is therefore highly needed.

1.4.2 Stellar properties of Herbig stars

Herbig stars are the bridge between low and high mass star formation. Due to their higher stellar mass compared to T Tauri stars, there are stark differences with respect to their stellar and disk evolution. Herbig stars are more luminous and have higher effective temperatures, which result in Herbig stars having a higher UV radiation field, impacting the chemistry differently (see, e.g., Jonkheid et al. 2007, Miotello et al. 2016). This higher UV emission for example results in warmer disks resulting in less chemically complex carbon-bearing molecules (Bosman et al. 2018; Agúndez et al. 2018). Their higher mass also means that their evolution towards the main sequence occurs quicker when compared to T Tauri stars. This is especially the case for Herbig Be stars. Based on near infrared excess Vioque et al. (2018) found that the disks surrounding the Be stars are typically smaller for stars with a mass more than 7 $M_\odot$ than their lower mass counterparts, which is likely due to their stronger UV emission. Herbig Be stars are also found to be more clustered compared to the lower mass Ae stars (Vioque et al. 2023). As Herbig Be stars generally reside at larger distances from Earth, in combination with the fact that many of them are still surrounded by leftover cloud remnants, means that interferometer observations are needed to study them, which are still lacking (Brittain et al. 2023).

Accretion rates of Herbig stars are determined in the same way as is done for T Tauri stars. However, the accretion tracers are generally at UV wavelengths, where the Herbig star is brighter than a T Tauri star, making the contrast between the accretion luminosity and the stellar photosphere for Herbig stars smaller. This leads to a minimum accretion rate of $\sim 10^{-9}$-10^{-8} $M_\odot$ yr^{-1} (e.g., Mendigutía et al. 2011; Fairlamb et al. 2017; Wichittanakom et al. 2020; Grant et al. 2022). Some tracers of the accretion luminosity are for example Hα (Wichittanakom et al. 2020) and Brγ (Grant et al. 2022). Based on the line luminosity of these tracers the accretion luminosity can be determined via a linear relationship between the two, where the slope and intercept are different for each tracer (e.g., Fairlamb et al. 2017).

Once the accretion luminosity is determined one can obtain a mass accretion rate by assuming that the material is falling from infinity via

$$\dot{M}_{acc} = \frac{L_{acc} R_\star}{G M_\star}, \tag{1.5}$$

where L_{acc} is the accretion luminosity, $R_\star$ and $M_\star$ are respectively the stellar radius and mass, and G is the gravitational constant. The accretion onto T Tauri stars is thought to occur via the magnetic field lines of the star's magnetic field (e.g., Hartmann et al. 2016). As the outer layers of these lower mass stars are convective, a magnetic field is generated which truncates the disk, the gas from the disk free-falls along the field lines resulting in the kinetic energy being changed into UV luminosity. This is called the magnetospheric accretion (MA) paradigm.

However, as higher mass stars are expected to have radiative envelopes, which do not generate a magnetic field, MA may not be applicable for Herbig stars. Still, it seems like that it can be applied to Herbig stars, especially to Herbig Ae stars, as the relationship only changes from that of the T Tauri stars above a stellar mass of 4 $M_{\odot}$ (e.g., Wichittanakom et al. 2020). Magnetic fields have been detected towards a few Herbig stars (Alecian et al. 2013; Hubrig et al. 2015; Mendigutía 2020), which may be fossil in nature (Brittain et al. 2023).

1.4.3 Evolution of Herbig disks

Disks around Herbig stars have been the focus of many in-depth studies. One of the main properties of Herbig disks is the so-called Meeus group, first identified by Meeus et al. (2001). Based on the mid-to-far-infrared spectral energy distribution (SED) of 14 Herbig stars measured with ISO, Meeus et al. (2001) divided the Herbig disks into two separate groups: group I for which the near- and mid-infrared continuum could be described by a power-law and a blackbody, while the group II disks can be reconstructed with only a power-law. Sub-groups were implemented as well, where the 'a' suffix was added when solid state bands are present, and a 'b' suffix was added if those were not visible. Other works have quantified this definition by either using IRAS 12-60 μm color (van Boekel et al. 2005), or an IR flux ratio (Khalafinejad et al. 2016).

The interpretation of these groups has stayed relatively similar since they were defined. Meeus et al. (2001) themselves interpreted the two groups as being either flared (group I) or flat (group II) disks. This results in an increase in far-IR emission, and thus FIR excess, for the group I disks, as the outer parts of the disk are illuminated by the star. On the other hand, as the group II disk is flat, the outer disk is not irradiated leading to no FIR excess. Dullemond & Dominik (2004a) modeled the SED of group I and group II disks and showed that the flaring of the disk can explain the seen dichotomy in Herbig disks. Later, Honda et al. (2012) proposed that the group I disks are disks with an inner cavity depleted of material, which results in large inner walls contributing to the mid and far-infrared excess.

Based on mid-infrared imaging, Maaskant et al. (2013) refined this view by proposing that Herbig disks start as a full flaring disk which eventually either form a gap, resulting in a group I disk, or flatten, resulting in a group II disk. Depending on the location of the gap size, the region from which the solid state bands originate are either completely depleted or heavily irradiated resulting in the corresponding 'a' and 'b' sub-classification. This would also mean that if a group II disk were to create an inner cavity, there would be an influx of group II disks towards the group I disks (Maaskant et al. 2013; Menu et al. 2015).

The last few years some major refinements have been made to this idea. As both resolved continuum dust emission with ALMA and scattered light imaging with SPHERE became available, Garufi et al. (2017) noted that there are large group II Herbig disks in sub-millimeter continuum, while barely or not visible in scattered light. Group II disks can also be small and flat, resulting in the same SED classification. An interplay between the inner and outer disk was found by

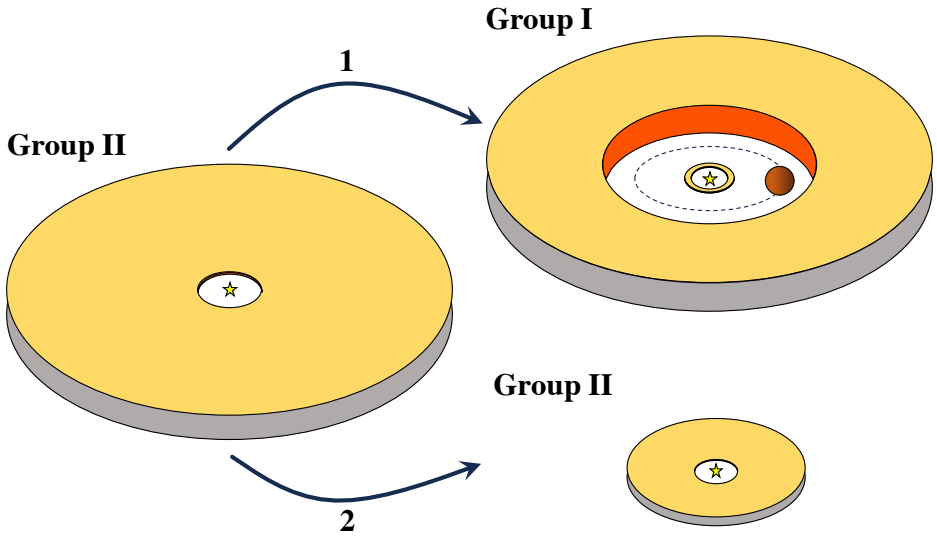

Figure 1.7: Proposed evolution of Herbig disks. First a full disk forms. Due to an puffed up inner disk the outer disk is shadowed, leading to a group II classification. Once a giant planet has formed in the outer disk, radial drift is stopped and an inner cavity forms, now depleted of dust (1). The inner rim of the disk is illuminated by the central star giving rise to a group I classification. In some disks a giant exoplanet does not form in the outer disk, leading the disk to shrink over time and stay classified as a group II (2).

Garufi et al. (2022): if the size of the disk seen in scattered light is small, but the NIR excess is large, the group II disk is shadowed by the inner disk, but if the disk does not have a large NIR excess, the group II disk is simply small. On the other hand, group I disks are generally large in both continuum emission and scattered light, with a clear gap visible in the continuum emission. If an inner disk is present in a group I disk this can shield the inner cavity from UV radiation and CO can survive (Banzatti et al. 2018).

Hence, the following intriguing picture arises. A full disk forms around a star, in which planets are forming. As the inner disk can still be puffed up, the outer disk is not irradiated by the central star. Once a massive planet forms, the radial transport of solids is stopped at the inner edge of the outer ring. The inner disk clears out due to radial drift and an empty inner cavity is formed; the outer disk now gets irradiated by the central star. On the other hand, if a massive planet does not form, the disk shrinks over time as all of the mass is accreted onto the star. The large group II disks could therefore still be able to evolve towards a group I classification by emptying an inner cavity. Similar scenarios have been proposed based on the morphology of disks around lower mass stars (van der Marel et al. 2018; Cieza et al. 2021).

It should be noted that the complexity needed to explain the group I and

group II classification should possibly incite us to rethink this classification. As high resolution observations of Herbig disks are now available, group I disks show deep cavities, while group II disks do not, with some exceptions. A redefinition would therefore simply be that group I disks are those with a cavity, or the transitional disks, while the group II disks are those without. More high resolution observations, especially for the more compact disks, are therefore highly needed.

1.4.4 Planet formation leftovers

After the Class II phase of the Herbig disks has passed, a debris disk is left over. Debris disks need to be sustained by collisional processes, and are therefore also known as secondary disks (Hughes et al. 2018). Debris disks around intermediate mass (AB-type) stars are found to have a higher detection rate of CO at millimeter wavelengths compared to later (FGK) spectral type stars (Lieman-Sifry et al. 2016). Though, a large range in upper limits is found, many at a similar level as the detections around AB-type stars (Matrà et al. 2015; Hughes et al. 2018). Both the origin of the gas (either primordial or second-generation) and the reason why there is a higher detection rate around intermediate mass stars is still heavily debated (Hughes et al. 2018). Additionally, a large fraction of the pre-main sequence intermediate mass stars with an infrared-excess are debris disks (Iglesias et al. 2023).

Going to the final result of planet formation, the exoplanets themselves, many thousands of exoplanets have been found to date and show a dependence on stellar mass. A large fraction of exoplanets consist of smaller planets such as super-earths residing around lower mass stars (e.g., Mulders et al. 2015), and, as discussed previously, may be related to the compact non-substructured disks. On the other

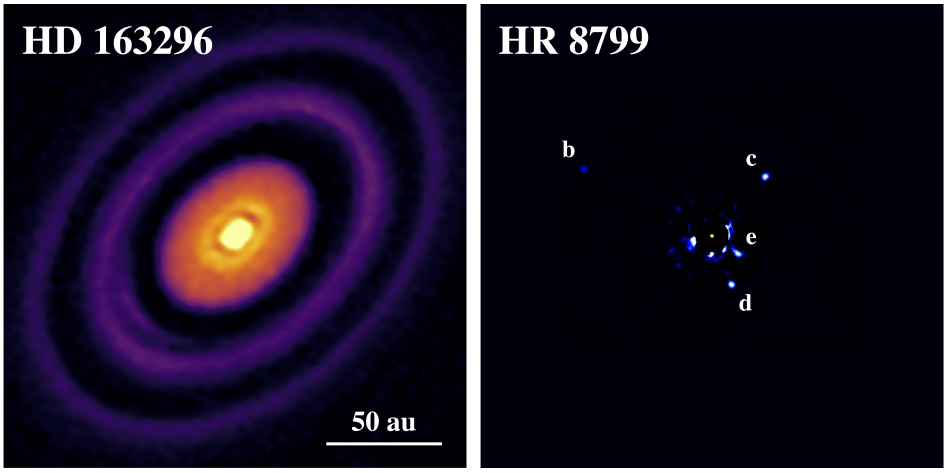

Figure 1.8: The spatial scales of the HD 163296 Herbig disk and the HR 8799 planetary system are remarkably similar (Andrews et al. 2018a; Marois et al. 2008, 2010). We may be witnessing the birth of a similar planetary system as HD 8799 in HD 163296.

hand, the occurrence rate of giant planets increases with stellar mass and is highest around intermediate mass stars (1.5-2 $M_{\odot}$, e.g., Johnson et al. 2007, 2010; Reffert et al. 2015; Nielsen et al. 2019). As mentioned before, the number of disk substructures is likely related to this (van der Marel & Mulders 2021), although this does invoke planet migration to occur for giant planets from the outer regions of the disk inwards. Yet, direct observations of exoplanets further away from their host star show that giant planets around intermediate mass stars such as HR 8799 (Marois et al. 2008, 2010), β Pic (Lagrange et al. 2010), and 51 Eri (Chauvin et al. 2017), are common (Vigan et al. 2021). The spatial scale of the HR 8799 system, consisting of four giant planets (7-10 $M_{\rm jup}$) at tens of au in separation, is very similar to that of HD 163296 (see Fig. 1.8). Observing planet formation occurring in the disk itself is more difficult, but over the last few years methods (in)directly detecting planets have started to be fruitful: PDS 70 (Keppler et al. 2018), AB Aur (Currie et al. 2022), HD 169142 (Hammond et al. 2023), HD 163296 (Izquierdo et al. 2022), HD 100546 (Booth et al. 2023a), AS 209 (Bae et al. 2022), and HD 97048 (Pinte et al. 2018b). Most of these detections are around intermediate mass stars.

These giant exoplanets are also influencing the elemental makeup of the central star itself. At least 33% of Herbig stars are found to be depleted in refractory elements, compared to 2% of all field stars (Folsom et al. 2012; also known as the λ Boötis phenomenon, Morgan et al. 1943). Herbig stars hosting group I disks are found to be depleted in refractory elements by 0.5 dex, but not in volatile elements, while Herbig stars hosting a group II disk are not depleted (Kama et al. 2015; Guzmán-Díaz et al. 2023). As group I disks are known to have large cavities (Fig. 1.7), this depletion of refractory elements of their host stars may point towards giant-planets forming in their disks.

Considering that current facilities are limited to detecting (proto)planets down to only a few Jupiter masses, Herbig disks are going to be one of the most important group of objects to hunt for giant planets and understand their formation. Systematic high spatial resolution studies are therefore urgently needed.

1.5 This thesis

The last decade, ALMA has observed complete star-forming regions, which almost primarily consist of T Tauri stars. As a consequence, a systematic study on disks surrounding higher-mass stars has mostly been ignored. This in spite of some of the most well-known and well-studied disks residing around Herbig stars. This thesis therefore focuses on the Herbig disks, and investigates how these compare to T Tauri disks. This thesis primarily aims to obtain a systematic view of the mass content in and radial extent of Herbig disks; both based on the dust and gas observations. This goal is primarily achieved with the use of archival data of the ALMA interferometer. The recent Gaia updated parallaxes have allowed for a much better determination of the Herbig star population, resulting in multiple works obtaining updated stellar parameters and distances for all known Herbig stars (e.g., Vioque et al. 2018; Guzmán-Díaz et al. 2021). Based on these works

all archival Band 6/7 ALMA data are obtained to determine the dust mass and radius from the continuum emission, gas mass and radius from the CO isotopologue emission, and compare the radial and vertical heights to infer evolutionary scenarios. The main work of this thesis is summarized in the following chapters.

Chapter 2 obtains the dust masses of Herbig disks, by obtaining archival Band 6 and Band 7 ALMA data of 36 Herbig disks. This results in a 64% complete sample out to 225 pc, and 38% complete out to 450 pc of the Vioque et al. (2018) sample. Comparing the obtained dust masses to those of the Lupus and Upper Sco star-forming regions, Herbig disks are found to be a factor of ~ 3 and ~ 7 more massive respectively. Moreover, while not all disks are resolved in these data, the Herbig dust disks are found to be larger in size compared to T Tauri disks. Differentiating between the group I and group II SED classification shows that the group I disks are more massive than the group II disks. As intermediate mass stars are associated with a high occurrence rate of giant planets, this difference in dust masses between the T Tauri and Herbig disks, and the differences between the group I and group II disks in the Herbig disk population itself, could be related to giant planet formation. As radial drift is stopped in the Herbig group I disks, the subsequent disk evolution then enlarges the differences between the T Tauri disks (or group I and group II disks) resulting in enlarging the inferred disk masses.

Chapter 3 focuses on the gas masses of Herbig disks, which is in effect the total disk mass and important for setting the stage of planet formation in disks. Multiple techniques have been developed to determine the total mass of a disk in the past years, one of which is with the use of the CO isotopologues ^{13}CO and C^{18}O. While for T Tauri stars CO has been shown to be frozen out and reprocessed into other molecules, resulting in apparent low gas masses, Herbig disks are expected to be much warmer, and hence the total mass can be determined by using CO. This chapter gathers the ^{12}CO, ^{13}CO, and C^{18}O observations of 35 Herbig disks, consisting of ALMA archival data and new NOEMA observations. Using the thermochemical code Dust And LInes (DALI), the luminosity of the CO isotopologues can be related to the total disk mass. It is found that the Herbig disks are optically thick in both the ^{13}CO and C^{18}O isotopologues, resulting in lower limits on the total disk mass for most of the 22 disks in which the two isotopologues are detected. Combining with the dust masses from Chapter 2, the gas-to-dust ratios are found to be consistent with 100 (the canonical interstellar matter value) or higher. Over multiple orders of magnitude in dust mass, the gas-to-dust ratio is two orders of magnitude higher compared to those found for T Tauri disks with similar techniques, indication the importance of the chemical conversion of CO in colder T Tauri disks.

Chapter 4 presents the first complete survey of Herbig disks in a single star-forming region. A total of 35 Herbig disks are identified in the Orion region, of which this chapter presents 25 new NOEMA observations and an additional 10 ALMA archival data. These data are used to obtain an unbiased view of the dust masses around Herbig disks. A median dust mass of 11.7 $M_\oplus$ is found, hence

around 50% of the Herbig disks are more massive than 10 $M_\oplus$ while this is only the case for less than 25% of the T Tauri disks in Orion. Comparing these dust masses to those found in Chapter 2, a slight bias towards higher disk masses is found for the disks observed with ALMA compared to those in Orion. Moreover, due to the higher dust masses specifically at the lower UV-irradiated regions, a steeper relation between the dust mass and UV irradiation is found compared to T Tauri disks.

Chapter 5 combines the dust masses from Chapter 2 together with accretion rates of Herbig disks to obtain the disk mass accretion rate relationship for Herbig disks. This fundamental property has been well-established for T Tauri disks, and is a key diagnostic in constraining the disk lifetime. For a total of 32 Herbig disks both parameters are known, and while the accretion rates are largely flat around 10^{-7} $M_\odot$ yr^{-1}, the dust masses differ over three orders of magnitude in dust mass. Specifically around the high dust mass end the Herbig disks follow the established T Tauri disk relationship. The problem arises from the 12 outliers at low dust mass high accretion rates, for which a disk lifetime of less than 0.01 Myr is inferred, most of which are group II sources. As Herbig stars need a high accretion rate to be identified as such, these objects have likely been identified in part by this bias. Multiple solutions are proposed, from optically thick dust emission, to overestimating the accretion rate due to disk winds contributing to the Brγ line. Still, the data suggests that group II disks are on the verge of dissipation, which may be due to efficient radial drift in these disks as they were not able to form dust traps in the outer disk like group I disks.

Chapter 6 explores the interpretation of group I disks being vertically extended, while group II disks are flat or self-shadowed by directly tracing the emission height of eight Herbig disks in ^{12}CO. All four group I disks are found to be vertically extended, while the four group II disks are either vertically extended or compact ($<$ 200 au in size) and flat. These findings agree with previous works, suggesting that group II disks can be either shadowed, but still large, or small and flat. The two group II disks which are found to be vertically extended (MWC 480 and HD 163296) may be precursors of group I disks, which will eventually form a cavity and the outer disks starts to be irradiated. The two flat disks (AK Sco and HD 142666) may have undergone significant settling because of the advanced age of the disks.

Chapter 7 looks into the disks of the precursors of Herbig stars, the Intermediate mass T Tauri (IMTT) disks. Obtaining ALMA archival data of 34 IMTT disks, the dust and gas masses are obtained using the techniques from Chapters 2 and 3. The IMTT disks are found to have the same dust and radius distributions as the Herbig disks. Furthermore, no differences in dust mass are found between the group I and group II disks, which further substantiates the hypothesis proposed in Chapter 2 where group I disks have formed a giant exoplanet stopping radial drift, while the group II disks have not and slowly drift towards smaller and more optically thick disks. Based on these findings, it is concluded that most disks around intermediate mass pre-main sequence stars converge quickly to small disks

unless prevented by a massive exoplanet.

The following main conclusions can be constructed based on the chapters of this thesis:

1. Herbig disks are massive, both in dust and gas (*Chapters 2-4, 7*).
2. The Herbig dust masses are more massive compared to T Tauri disks, especially when taking the advanced age of the Herbig disks into account compared to the younger T Tauri disks (*Chapters 2, 4*).
3. Herbig disks are larger in size compared to T Tauri disks (*Chapter 2*).
4. For the warmer Herbig disks CO freeze-out is not significant, in contrast to the colder T Tauri disks, resulting in CO being a good disk mass tracer in these disks (*Chapter 3*).
5. Herbig disks are found to have high accretion rates independent of disk dust mass, which is in contrast to T Tauri disks for which a positive correlation is found (*Chapter 5*).
6. The group I, group II classification of Herbig disks may need to be redefined, now that resolved high-resolution millimeter observations are available (*Chapters 2, 6*).
7. Giant planet formation is impacting the evolution of Herbig disks. The high disk masses and large radii (*Chapters 2, 3, 7*), the quick or slow dissipation of the disk (*Chapters 2, 5*), the significant differences compared to T Tauri disks (*Chapters 2, 4*), and the similarities between the disks around Herbig stars and the disks around their precursors the IMTT stars (*Chapter 7*), are all pointing towards giant planet formation occurring in these disks.

1.6 Future outlook

The future of Herbig stars and disks is bright. Following on the Chapter 2 results, a push towards obtaining a full set of millimeter observations of Herbig disks is now starting to be fruitful. In the near future a full dust mass study on all known Herbig disks within 750 pc will be possible. This will increase the number of Herbig disks with millimeter observations by a factor of more than 5 compared to the study done in Chapter 2. This will give great insights into the population of Herbig disks, with numbers comparable to many T Tauri disk dominated star-forming regions. The additional ALMA 2030 upgrades will allow for deeper observations in shorter integration times, and cover more molecular lines in a single observation, which is ideal for large population studies of disks.

In the coming years, a large part of the community will focus on observing protoplanets (in)directly in disks. As recent observations have shown, many of the directly and indirectly observed protoplanets in disks are around Herbig stars. As intermediate mass stars have a high occurrence rate of giant exoplanets, in

combination with a Jupiter mass sensitivity of the current observatories, Herbig disks will be at the forefront of understanding the formation and evolution of giant exoplanets in the foreseeable future. One should also not forget the compact Herbig disks, which are in desperate need to have high resolution ALMA observations, to both obtain a measure of their size and search for substructures. These disks likely form Super-Earths due to the higher pebble flux. Upcoming large telescopes such as the Extremely Large Telescope (ELT) will therefore be important in observing the inner regions of these disks and look for lower mass planets. This necessitates obtaining high resolution and deep ALMA observations of all Herbig disks.

For tracing the total mass in Herbig disks, rare CO isotopologues such as $^{13}C^{17}O$ will be important. With ALMA these should be detectable in a large fraction of the Herbig disk population within an hour of integration time. While HD is still thought to be one of the best disk mass tracers, there will not be any observatories which will be able to observe the $J = 1 - 0$ line soon. One of the planned far-infrared probes, the Space Infrared Telescope for Cosmology and Astrophysics (SPICA), has unfortunately been discontinued. Still, for Herbig disks there are a dozen HD upper limits available to combine with the rare CO isotopologues. Regarding the dust, the upcoming Square Kilometer Array (SKA, Ilee et al. 2020) and the Next Generation Very Large Array (ngVLA) will revolutionize our understanding of cm-sized grains (provided that processes such as free-free emission can be accounted for), and give insights into if the disks are optically thick.

Especially for probing the group I and group II dichotomy in Herbig disks, tracing the inner disk will be of importance. The James Webb Space Telescope (JWST) is already revolutionizing our understanding of the inner disk chemistry of mostly T Tauri disks, as nearby Herbig disks are too bright. Still, the influence of the outer disk on the composition of the inner disk will be interesting to test in the context of the two groups. Later on, ELT will advance this further. Regarding scattered light imaging, the Spectro-Polarimetric High-contrast Exoplanet REsearch (SPHERE) instrument on the Very Large Telescope (VLT) is close to being decommissioned, but the improved contrast of SPHERE+ will especially be important for the bright Herbig stars, to probe the smaller or shadowed disks in the population.

Lastly, and more practically, as also mentioned in Brittain et al. (2023), the definition of what a Herbig star is may need to be reassessed. The current definition includes only pre-main sequence intermediate mass stars with hydrogen emission line features, likely biasing the population to high accretors. Ideally the definition should include all pre-main sequence stars with stellar masses of $1.5 - 10$ $M_\odot$.

Concluding, there is much to be looking forward to the coming years, not only in the field of Herbig stars and disks, but in the general field of planet formation.